Persistent Noise Signal in the FairfieldNodal Three-Component 5-Hz Geophones

by Jamie Farrell, Sin-Mei Wu, Kevin M. Ward, and Fan-Chi Lin

ABSTRACT

Data from deployments of the FairfieldNodal three-component nodes were used to analyze a persistently observed noise signal. The noise signal is most prominent in the 20- to 40-Hz range but has been observed anywhere in the 10- to 100-Hz range. Interestingly, the signal is affected by air temperature and moves to higher frequencies in colder temperatures. Nodes that were deployed in seismic vaults directly on flat concrete slabs do not show the noise signal, and nodes that were buried in the ground or covered in snow show a significant decrease in the noise signal. This suggests that whatever is causing this signal may be mitigated by better coupling to the ground. Spectral analysis of hydrothermal tremor in the Upper Geyser Basin, Yellowstone, suggests this noise signal can interfere with the true ground vibration and can impede the ability to accurately characterize these signals. It is our recommendation to always bury the nodes if it is possible to reduce this noise signal that can interfere with natural signals of interest in a similar frequency band. In addition, tests to better estimate the best gain setting were done, and results show that above 12 dB, the waveforms of teleseismic events on the three-component nodes are very similar, suggesting that there is no advantage to using a gain setting higher than 18 dB for recording teleseismic events. If background noise is of interest in addition to teleseismic events, we see no adverse effects on the waveforms of teleseismic events using the max gain setting of 36 dB.

INTRODUCTION

With the advancement of newer, smaller, less expensive, and fully autonomous seismic sensors, larger and denser seismic experiments are becoming more commonplace. These sensors have been primarily developed for the oil and gas industry, but academic and research institutions are using them more and more for large-*N* experiments (> 100 instruments). Discussed in this article is the use of the three-component FairfieldNodal Zland, Generation 2 seismometers (hereafter called nodes). One big advantage of these nodes is that they are cable free (Freed, 2008), making it easier and faster to deploy the instruments in any manner and geometry (Hand, 2014). In addition, they are fully autonomous, meaning that everything is within the roughly 11.7-cm diameter and 16.3-cm-high enclosure, including three geophones, a rechargeable lithium-ion battery, a data logger, and a Global Positioning System clock.

Previous works using the new 5-Hz, three-component nodes included deployments in Yellowstone (Ward and Lin, 2017; Wu *et al.*, 2017), Utah (Ward and Lin, 2017), and Oklahoma (The Incorporated Research Institutions for Seismology [IRIS] Community Wavefield Experiment, Anderson *et al.*, 2016). Prior to that, there were many experiments using the previous 10-Hz, vertical-component nodes including deployments in Long Beach, California (Lin *et al.*, 2013; Schmandt and Clayton, 2013); Mount St. Helens, Washington (Hansen and Schmandt, 2015; Wang *et al.*, 2017); and the San Jacinto fault zone, California (Ben-Zion *et al.*, 2015). In addition to numerous academic institutions that have recently purchased three-component nodes, the IRIS Program for the Array Seismic Studies of the Continental Lithosphere (PASSCAL) instrument center has 63 three-component nodes, which are available to researchers on a first-come, first-served basis.

Here, we focus on using data from three different deployments of three-component nodes (Fig. 1) to show the observed noise signal that is common to all these deployments. The goal is to identify and document this instrument or coupling noise for the purpose of separating it from real signals of interest. Data will be shown from (1) deployments around Old Faithful in the Upper Geyser Basin of Yellowstone National Park, Wyoming (Ward and Lin, 2017; Wu *et al.*, 2017); (2) a deployment of eight nodes (Ward and Lin, 2017) near station NLU, a permanent broadband instrument located in the East Tintic Mountains near Eureka, Utah, operated by the University of Utah Seismograph Stations (University of Utah, 1962); and (3) a deployment of 16 nodes in eastern Salt Lake City (FCL) to test how burying the nodes would affect the noise signal.

Spectrograms for each station were calculated using the method of Koper and Hawley (2010) and Xu *et al.* (2017) in the following manner for stations with a 1000-Hz sampling rate:

1. The instrument response of each component was removed by spectral division in the frequency domain using a trapezoidal taper defined by frequencies of 0.025, 0.050, 400, and 500 Hz, resulting in records of ground acceleration with units of m/s^2.
2. Each hour-long trace of 3,600,000 samples was divided into 20 subwindows of 439,000 samples (439 s) that overlapped one another by ~62%. Each subwindow was

doi: 10.1785/0220180073

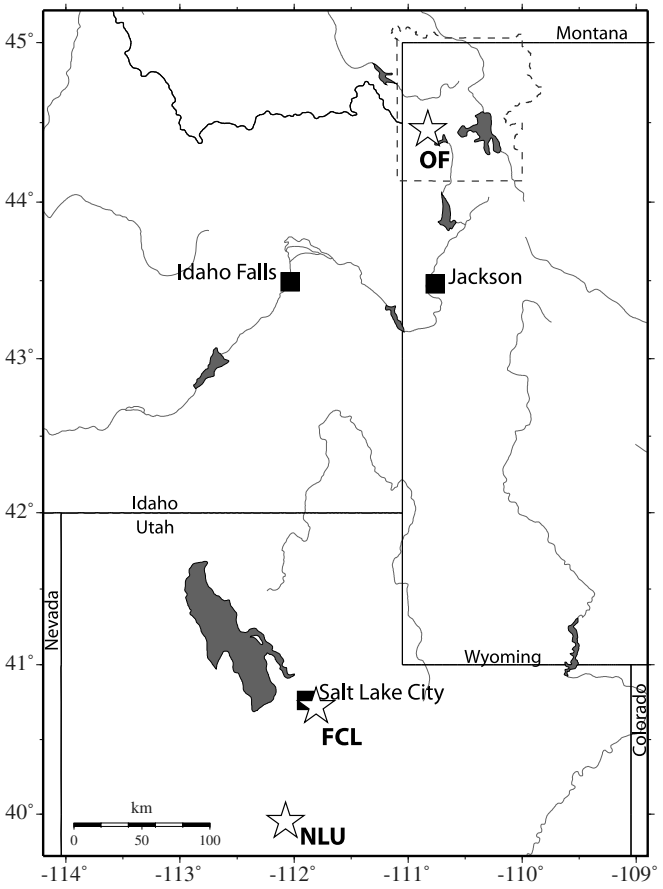

▲ **Figure 1.** Map showing the locations of seismic deployments discussed in the Introduction (white stars). Black squares represent population centers in the region. Light gray lines represent rivers, and dark gray polygons represent bodies of water. Bold black lines represent state boundaries, and the dashed black line represents Yellowstone National Park.

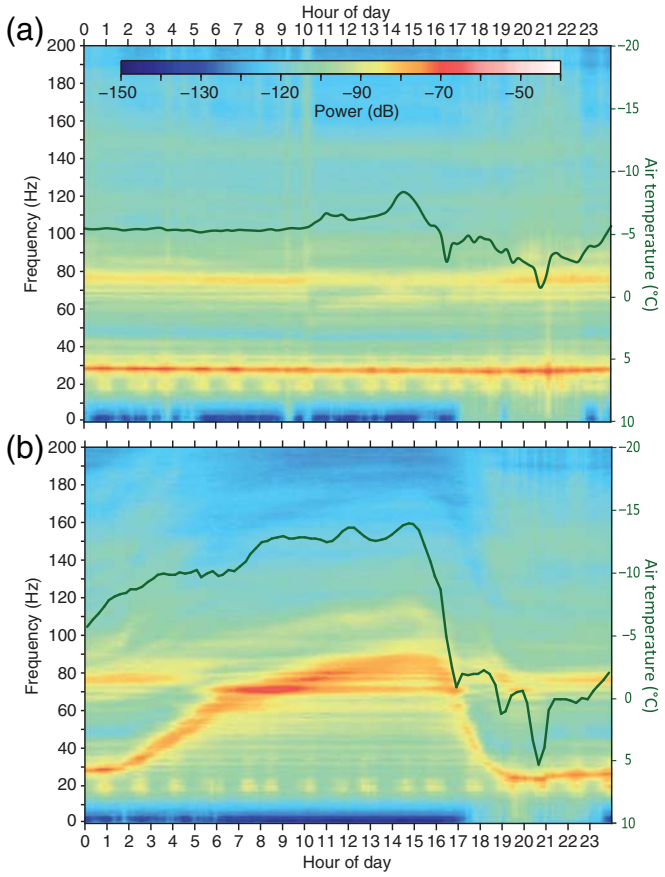

▲ **Figure 2.** Twenty-four-hour spectrograms of a nodal seismic station (east–west component) in Yellowstone National Park on (a) 6 November 2015 and (b) 7 November 2015 showing the persistent noise signal (a) and how it is affected by changes in air temperature (b). Power is measured relative to ground acceleration in decibel (dB) units of $10\log_{10}(m^2/s^4/Hz)$. All times are in UTC.

detrended, and a Nutall4c taper (Heinzel *et al.*, 2002) was applied.

3. In each subwindow, fast Fourier transforms (FFTs) were calculated, and the corresponding 3-by-3 frequency-dependent spectral matrix was calculated by multiplying the FFT of each component by the complex conjugate of the FFT of each component.
4. The spectral matrices for each subwindow were normalized and time averaged into a single spectral matrix for the hour-long segment of data. The spectral matrices were then frequency averaged into bins, ranging from 0.01 to 400 Hz.

For station NLU with a 100-Hz sampling rate, the process was the same except the trapezoidal taper was defined by frequencies of 0.025, 0.050, 40.0, and 50.0 Hz.

NOISE OBSERVATIONS

Beginning in November 2015, the University of Utah deployed an array of three-component nodes in the Upper Geyser Basin of Yellowstone National Park focused on Old Faithful Geyser (OF in Fig. 1). This array was deployed during 2–14 November 2015 and consisted of 133 nodes with an average station spacing of ~50 m and an ~1-km aperture (Ward and Lin, 2017; Wu *et al.*, 2017). Because of restrictions on digging in the sensitive hydrothermal area, all instruments were spiked into the ground on the surface. Many different signals were observed related to the various hydrothermal features in the basin. However, a persistent signal was observed at almost all stations dominantly at 20–40 Hz (Fig. 2a). Interestingly, this signal seems to be influenced by air temperature as it increases in frequency with decreasing air temperature (Fig. 2b). Notably, not all stations show the same noise signal, with some showing it in different frequency ranges, even if they are located near each other. In addition, each station responds differently to changes in air temperature, and there does not seem to be a predictable change in the noise signal as the air temperature decreases. Additional deployments in Yellowstone in 2016 and 2017 showed similar observations at mostly all

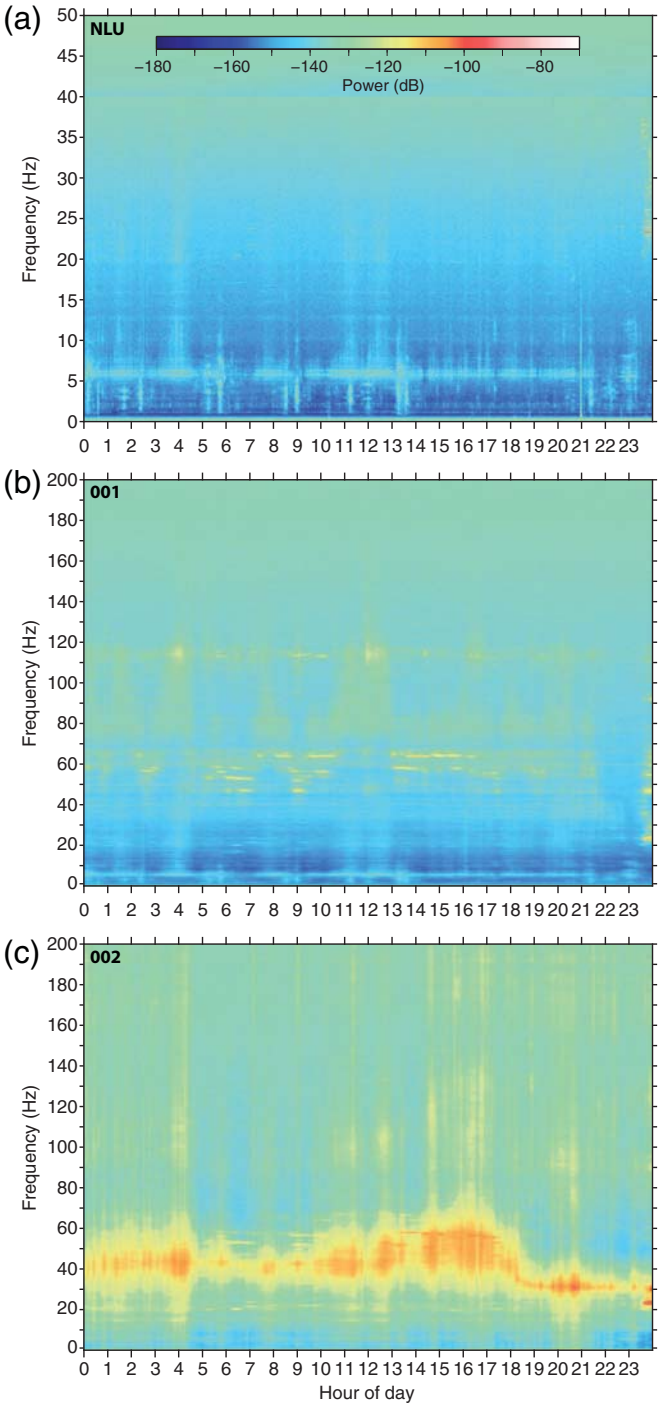

▲ **Figure 3.** Twenty-four-hour spectrograms of three seismic stations (east–west component) deployed in central Utah. (a) Station NLU, a permanent broadband station located in a seismic vault. (b) Nodal station 001 collocated with broadband station NLU within the seismic vault and placed on a flat concrete slab. (c) Nodal station 002 spiked into the surface directly above the seismic vault. Power is measured relative to ground acceleration in dB units of $10\log_{10}(m^2/s^4/Hz)$. All times are in UTC.

▲ **Figure 4.** Photo of deployment of nodal seismometers in Salt Lake City with seven collocated pairs of surface and buried nodes (red circles) with different gain settings.

stations deployed. The noise signal is higher in amplitude on the horizontal components by about 10%. Of all 133 stations deployed in the Upper Geyser Basin on 6 November 2015 (where the temperature was as low as ~ -15°C), the mean frequency of the noise signal is 31.4 ± 7 Hz with a power of -83.1 ± 9.7 dB on the horizontal channels and power of -90.6 ± 10.7 dB on the vertical channels. Power is measured relative to ground acceleration in decibel (dB) units of $10\log_{10}(m^2/s^4/Hz)$.

To verify that this was not a natural signal, we looked at data from other deployments in the western U.S. In January 2016, the University of Utah collocated eight nodal instruments with the permanent broadband station NLU (NLU in Fig. 1) of the Utah Seismic Network (University of Utah, 1962), mainly to test the viability of using the nodal instruments to calculate receiver functions (Ward and Lin, 2017). Station 1 was located within the vault and was placed on the concrete pad next to the broadband instrument at NLU. Station 2 was located on the surface directly above NLU and station 1. Stations 3–8 were located on the surface in a ring around station 2, each about 100 m from station 2. A spectrogram for the east component of station NLU on 23 January 2016 shows that it is quiet in the 25- to 50-Hz range (Fig. 3a). Similarly, nodal station 1, which was collocated with NLU in the vault on the concrete pad, is also quiet in the same frequency range (Fig. 3b). However, nodal station 2, which was located on the surface directly above these two quiet sensors, shows energy during the entire day in the 25- to 50-Hz range (Fig. 3c).

In addition, we looked at data from a deployment we did in Salt Lake City (FCL in Fig. 1) in December 2017 in which we deployed 16 nodes for around one month. Seven of the nodes were deployed on the surface with another seven buried about four inches deep right next to them (Fig. 4). Each pair of surface and buried nodal stations had a separate gain setting ranging from 0–36 dB in 6-dB increments. The difference in the noise

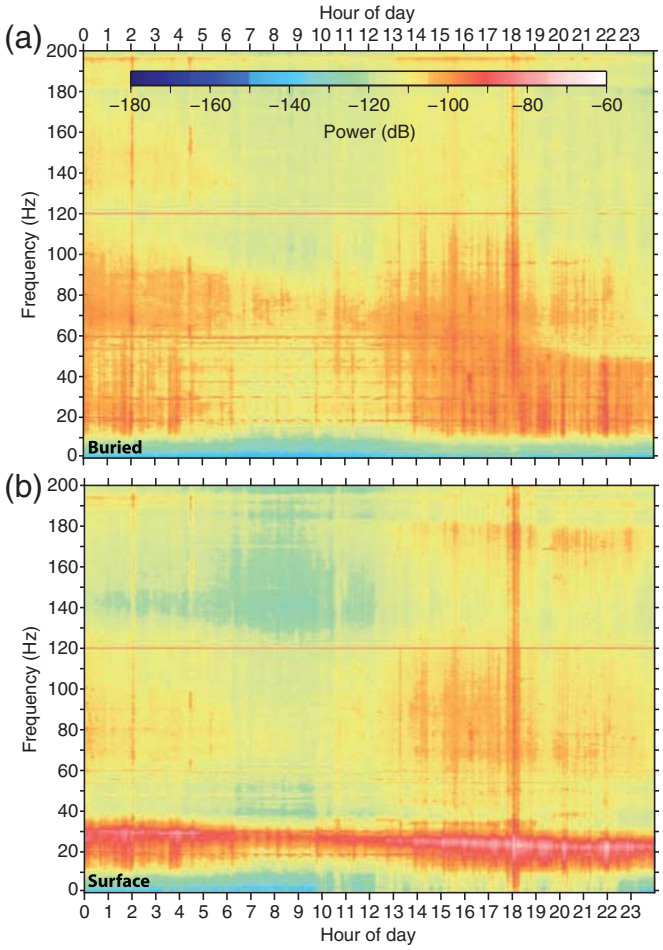

▲ **Figure 5.** Twenty-four-hour spectrograms of collocated nodal seismometers (east–west component). (a) Buried nodal seismometer and (b) surface spiked nodal seismometer. Power is measured relative to ground acceleration in dB units of $10\log_{10}(m^2/s^4/Hz)$. All times are in UTC.

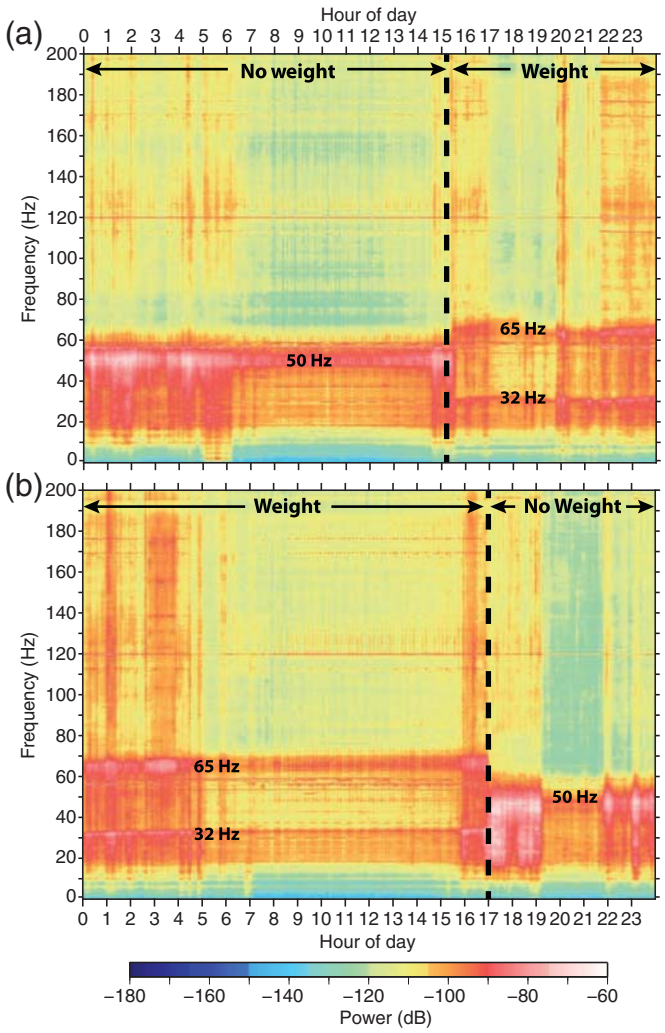

▲ **Figure 6.** Twenty-four-hour spectrograms of surface spiked nodal seismometer (east–west component) on (a) 8 November 2017 and (b) 9 November 2017. The 11-kg weight was placed on top of the node at around 15:20 UTC on 8 November 2017 and was removed around 17:00 UTC on 9 November 2017. Power is measured relative to ground acceleration in dB units of $10\log_{10}(m^2/s^4/Hz)$.

spectra can be seen in Figure 5, in which a spectrogram for 20 December 2017 for a buried node (Fig. 5a) and a collocated surface node (Fig. 5b) is shown. The noise signal is clearly visible in the surface node (Fig. 5b) in the 20- to 40-Hz range but is not discernable on the buried node (Fig. 5a). This pattern was the same with all six other pairs of nodes in the experiment.

An additional node was placed on the surface and spiked into the ground. An ~30-cm-high 11 kg weight was placed on the node to see how this would affect the observed noise signal. Results show that the surface node recorded a steady ~50-Hz noise signal that changed when the weight was added (Fig. 6). After the weight was added, the noise signal was much more complicated in that it split into two separate branches with one moving to higher frequencies at ~65 Hz and one moving to lower frequencies at ~32 Hz. After the weight was removed, the noise signal returned to ~50 Hz (Fig. 6). This removes the possibility that the observed noise is due to internal mechanical or electronic instrument vibrations because the ~11-kg weight did not change anything inside the instrument. In addition, these results indicate that the observed signal is not coming from the Earth but is related to the instrument because adding a weight on the instrument should not affect a natural signal either coming from below or from wind. One possibility for the change in the noise signal is that the weight changed the natural frequency of the node by adding length to it. Another possibility is that the additional ~11-kg weight better coupled the node to the ground, which then affects the natural frequency.

GAIN OBSERVATIONS

To date, no best practices have been established in the academic community regarding which gain setting (0, 6, 12, 18, 24, 30, and 36 dB) for this specific instrument is

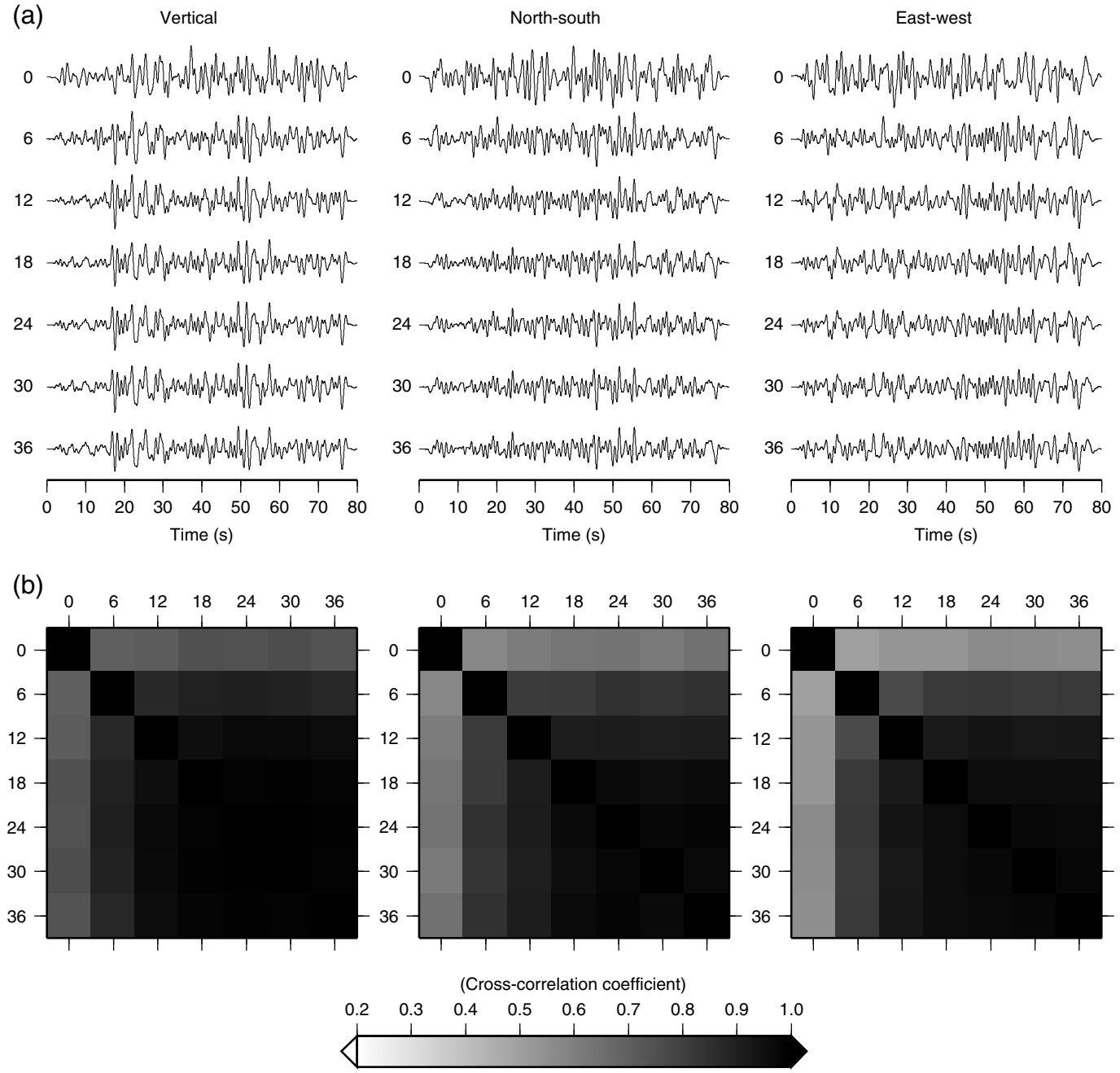

▲ **Figure 7.** Waveform characteristics and cross-correlation results from a teleseismic event recorded on seven nodal seismometers with varying gain settings. The recorded waveforms (a) are shown for all gain settings for the vertical (left column), north–south (center column), and east–west (right column) components. All waveforms have been filtered between 0.1 and 1 Hz. The cross-correlation coefficients between different gain settings (b) are also shown for the vertical (left column), north–south (center column), and east–west (right column) components.

appropriate resulting in arbitrary selections (e.g., pick the middle gain). A growing interest in using these instruments to record far-field sources (e.g., teleseismic events) motivated the deployment of seven collocated nodes. Each one of the nodes was deployed with a different gain setting to test how that setting affects the waveforms of teleseismic events. Specifically, we wanted to evaluate and quantify if there was a preferred gain setting for studies that only targeted teleseismic sources and if there were any trade-offs for studies that have a hybrid source target (e.g., local noise and teleseismic events). This would allow a more directed choice of the gain setting driven by the specific scientific target of the deployment.

A visual inspection of the waveforms from teleseismic events reveals considerable difference for the gain setting of 00 dB and to a lesser degree 6 dB (Fig. 7a). Above a gain setting of 12 dB, it is difficult to see a difference in the waveforms from

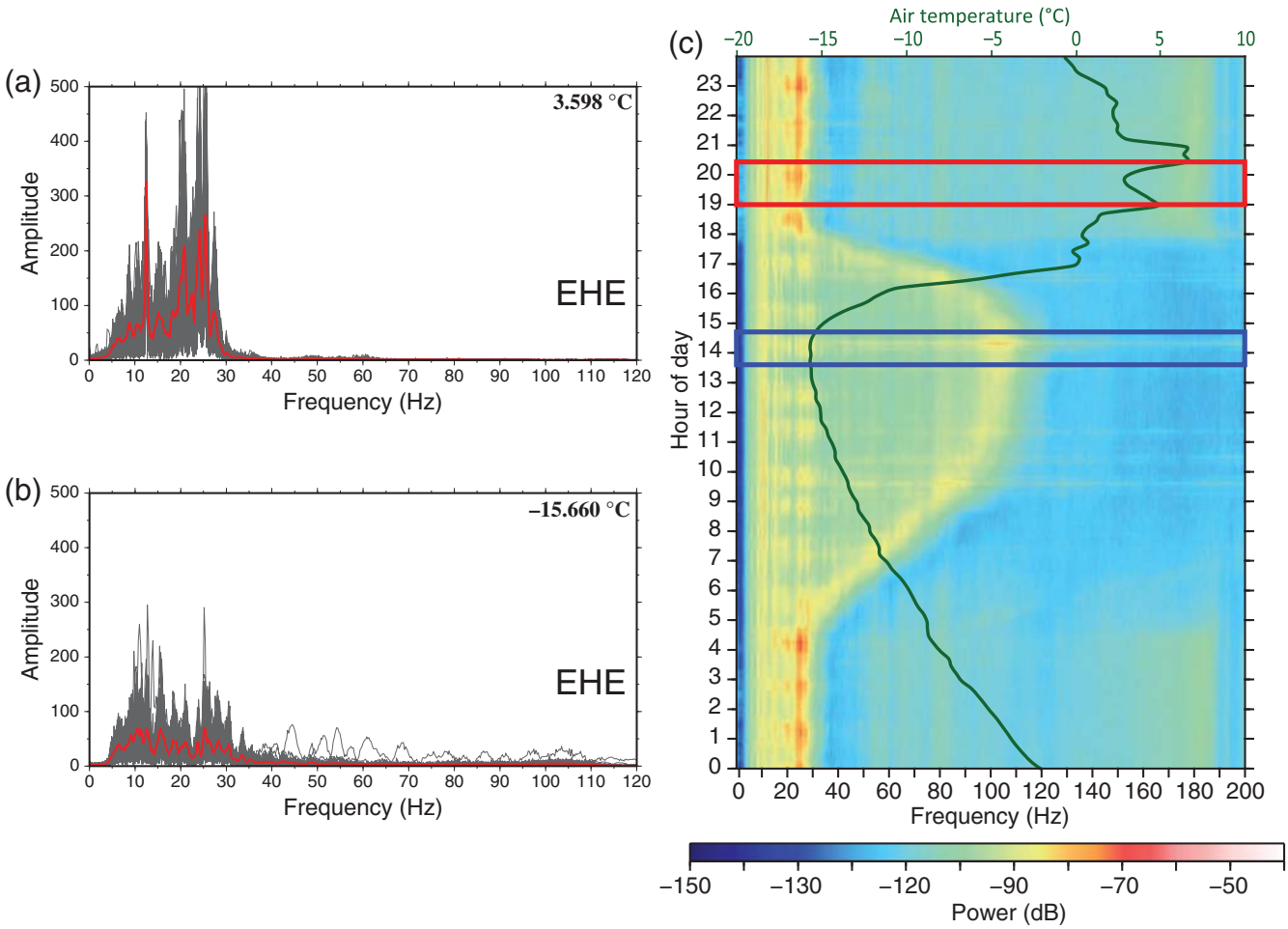

▲ **Figure 8.** Old Faithful tremor frequency characteristics of a nodal seismic station deployed near Old Faithful geyser in November 2015. (a) Noise characteristics for a relatively warm period corresponding to the red box in (c) (~19:02–20:25 UTC). (b) Noise characteristics for a relatively colder period corresponding to the blue box in (c) (~13:37–14:43 UTC). (c) Twenty-four-hour spectrogram for the same nodal station with variable air temperatures and noise signals. Individual gray lines in (a) and (b) represent normalized spectra from 3-s time windows that record Old Faithful tremor, and the red line represents the mean of the gray lines during the associated times in the red and blue box of (c), respectively. For (c) power is measured relative to ground acceleration in dB units of $10\log_{10}(m^2/s^4/Hz)$. All times are in UTC. All data are from the east–west component.

a simple visual inspection. To quantify the observed difference, we window a teleseismic event 15 s before and 65 s after the theoretical *P*-wave arrival and bandpass the waveforms between 0.1 and 1 Hz. Figure 7b shows the cross-correlation coefficient for each waveform against every other waveform. This pattern is similar for the majority of teleseismic events recorded during this deployment.

DISCUSSION

To show the potential of the observed noise to interfere with natural signals from the Earth, we examine data from the 2015 deployment in the Upper Geyser Basin of Yellowstone National Park (Ward and Lin, 2017; Wu *et al.*, 2017). About 45 min prior to eruptions of Old Faithful Geyser, there is an increase in intensity and amplitude of hydrothermal tremor. This tremor peaks in intensity and amplitude about 25 min prior to an eruption and decays to near background rates just before an eruption (Kedar *et al.*, 1996; Wu *et al.*, 2017). Here, we look at the dominant frequencies of these tremor packages during relatively cold and warm periods (red and blue boxes in Fig. 8c) to examine how the noise signal can interfere with natural signals. The size of the red and blue boxes was determined empirically and begin 15 min prior to the onset of tremor activity and end 10 min after an eruption of Old Faithful based on eruption timing from the GeyserTimes website (see Data and Resources). To calculate the noise spectra, we apply a detection method based on an adaptive short-term average/long-term average algorithm (Wagner and Owens, 1996; Withers *et al.*, 1998) to the continuous seismic data for Old Faithful eruption cycles in cold and warm times to isolate the events that make up the tremor packages (i.e., blue and red boxes in Fig. 8c, respectively). The detection windows are 3 s long based on observed tremor characteristics from the

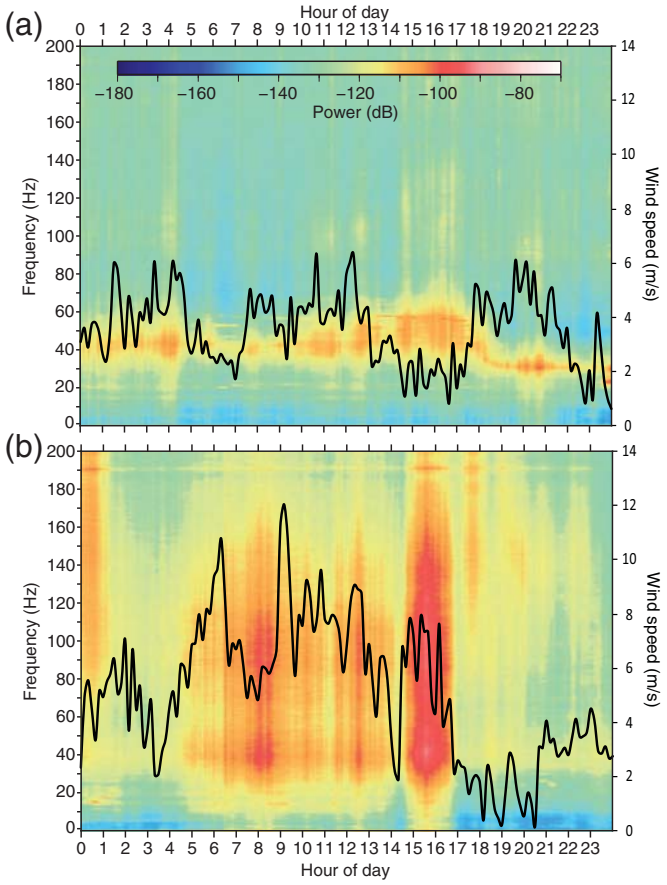

▲ **Figure 9.** Seismic signals due to wind. (a) Twenty-four-hour spectrogram (east–west component) for nodal station 002 (same as Fig. 3c) with wind speed shown as the black line at a nearby weather station on 23 January 2016 where the wind speed did not exceed ~6 m/s. (b) Twenty-four-hour spectrogram (east–west component) for the same station 30 January 2016 showing the seismic signal produced by high winds (black line) (up to ~12 m/s). Power is measured relative to ground acceleration in dB units of $10\log_{10}(m^2/s^4/Hz)$. All times are in UTC.

nodal stations located ~120 m from the Old Faithful vent. Figure 8a shows the frequency content (gray lines for each detection and red line for the mean of all detections) of the Old Faithful tremor during a relatively warm period (3.598°C) (red box in Fig. 8c) with high amplitudes in the 20- to 30-Hz range. However, in Figure 8b, which corresponds to a relatively cold period (−15.66°C) (blue box in Fig. 8c), we observe much lower amplitudes (gray lines for each detection and red line for the mean of all detections) in the 20- to 30-Hz range, which is the natural signal from Old Faithful tremor packages (Fig. 8b). During relatively warmer periods, the noise signal occupies the same frequencies and interferes with the natural Old Faithful tremor package in the 20- to 30-Hz range. During colder temperatures, the noise signal moves to higher frequencies (~100 Hz) and no longer interferes with the natural Old Faithful tremor signal. Although we cannot definitively determine the cause of this noise signal, we hypothesize that this amplification is due to resonance with the observed noise signal and not just the natural noise of the instrument because both the background noise level (when there is no Old Faithful tremor) and the Old Faithful tremor signal are amplified by about 75% during relatively warm periods.

In all the deployments of the three-component nodes by the University of Utah, we observed the noise signal in the range of 10–100 Hz with the most common range (normal temperature ranges, i.e., > −10°C) to be around 20–40 Hz. By looking at nearby weather stations, the noise signal does not correlate with wind speed and wind noise is distinct in that it encompasses a much wider range of frequencies similar to previous studies by Withers *et al.* (1996). Figure 9 shows spectrograms for two days for station 002 in the NLU deployment. On 23 January 2016, there was little wind recorded at weather station UTEUR (see Data and Resources) located about 2.4 km west-northwest of station NLU (Fig. 9a). In contrast, on 30 January 2016, a large wind event was recorded at UTEUR with an accompanying seismic signal observed from ~20–200 Hz (Fig. 9b). The wind noise is distinctly different from the noise signal that is of interest here. Parasitic resonance was investigated as a possible cause, but this tends to occur within the geophone when substantial amounts of seismic energy are present at frequencies more than an order of magnitude above the natural frequency of the geophone (Steeples and Miller, 1990), and we are seeing the noise signal at frequencies as low as 20 Hz on a 5-Hz corner geophone, so this is unlikely. Whatever the cause, there does seem to be a damping of the signal with better coupling to the ground. When the node was deployed in a vault and placed on a flat concrete slab on bedrock with better coupling, there was no noise signal observed (Fig. 3b). Similarly, when the node was isolated by being buried in the ground, the noise signal was greatly reduced and often absent all together (Fig. 5a). Similarly, when nodes were deployed on the surface and subsequently buried with snowfall, there was a noticeable decrease in the noise signal. The absence of the signal in the previous scenarios (seismic vault, buried in the ground, and covered in snow) could be attributed to increased thermal stability; however, a node buried 4 inches in the ground is not perfectly thermally insulated, so we believe this effect is minor compared with the increased coupling given that the noise signal is absent in this scenario. In all of our examples, the signal is around 10% stronger on the horizontal components than the vertical component when the signal is present on the vertical channel. However, there seems to be more to the noise signal than coupling alone as indicated by our dead weight test. When we placed the weight on top of the node to better couple it to the ground, the noise signal changed (shifted in frequency) but did not go away altogether.

CONCLUSION

A persistent noise signal most notably in the 20- to 40-Hz range (although it can span the 10- to 100-Hz range) is present in all nodal deployments by the University of Utah to date.

This noise signal is sometimes present on the vertical component but is higher in amplitude on the horizontal components by about 10%. The signal goes away entirely when the node is placed in a seismic vault and set on a flat slab of concrete. In addition, the noise signal is greatly reduced or is absent if the nodes are buried or if they are covered in snow. The amplification of the Old Faithful hydrothermal tremor signal suggests this noise signal can interfere with and amplify the true ground motion. We suggest that sensor coupling with the ground could potentially play an important role in the amplitude of this noise signal and thus recommend that nodes be buried in field deployments when possible. In addition, it seems that the noise signal is unique to each node because nodes that are near each other show different frequency noise signals and different responses to air temperature changes. This makes it very difficult to isolate the signal and remove it from each node in large-*N* deployments. Therefore, if higher frequency waveforms (10–100 Hz) are desired, it is our recommendation to bury the three-component nodes where possible.

Above a gain setting of 12 dB (18 dB for horizontal components), the waveforms of teleseismic events on the three-component nodes are very similar, suggesting that there is no advantage (disadvantage) to using a gain setting higher than 18 dB for recording teleseismic events. If, however, the target of the deployment has a hybrid source in which a gain of 36 dB might be better suited for local sources, we see no adverse effects on teleseismic events using this setting.

DATA AND RESOURCES

The seismic data from station NLU were from the Utah Seismic Network (UU), operated by the University of Utah. Data for station NLU were retrieved from the Incorporated Research Institutions for Seismology (IRIS) data center. Data from the University of Utah nodal deployments are available by contacting the author Jamie Farrell. The GeyserTimes website is available at www.geysertimes.org (last accessed June 2018), and weather conditions for station UTEUR are available at http://mesowest.utah.edu/cgi-bin/droman/meso_base_dyn.cgi?stn=UTEUR&unit;=0&timetype;=LOCAL (last accessed June 2018).

ACKNOWLEDGMENTS

Support was from the University of Utah Seismograph Stations, National Science Foundation (NSF) Grant Number CyberSEES-1442665, and the King Abdullah University of Science and Technology (KAUST) under Award OCRF-2014-CRG3-2300. The authors thank Andy Trow and David Drobeck for deploying nodal seismometers in the NLU experiment. Some nodes used in the Salt Lake City experiment were generously loaned to us by Amanda Thomas of the University of Oregon. Some nodes used in the 2015 Old Faithful experiment were generously loaned to us by Marianne Karplus of the University of Texas at El Paso and FairfieldNodal. The authors would also like to thank the Yellowstone National Park Center for Resources for providing the permit to work in Yellowstone and for providing personnel to help in the field. Figures were made using the public domain Generic Mapping Tool (GMT) software package (Wessel and Smith, 1991). The authors would like to thank Amanda Thomas and one anonymous reviewer for their constructive comments.

REFERENCES

Anderson, K., J. Sweet, and B. Woodward (2016). IRIS community wavefield experiment in Oklahoma, *Incorporated Research Institutions for Seismology, Other/Seismic Network*, doi: 10.7914/SN/YW_2016.

Ben-Zion, Y., F. L. Vernon, Y. Ozakin, D. Zigone, Z. E. Ross, H. Meng, M. White, J. Reyes, D. Hollis, and M. Barklage (2015). Basic data features and results from a spatially dense seismic array on the San Jacinto fault zone, *Geophys. J. Int.* **202,** 370–380, doi: 10.1093/gji/ggv142.

Freed, D. (2008). Cable-free nodes: The next generation land seismic system, *The Leading Edge* **27,** 878–881.

Hand, E. (2014). A boom in boomless seismology, *Science* **345,** no. 6198, 720–721, doi: 10.1126/science.345.6198.720.

Hansen, S. M., and B. Schmandt (2015). Automated detection and location of microseismicity at Mount St. Helens with a large-N geophone array, *Geophys. Res. Lett.* **42,** 7390–7397, doi: 10.1002/2015GL064848.

Heinzel, G., A. Rudginger, and R. Schilling (2002). *Spectrum and spectral density estimation by the Discrete Fourier transform (DFT), Including a Comprehensive List of Window Functions and Some New At-Top Windows*, 84 pp., http://hdl.handle.net/11858/00-001M-0000-0013-557A-5 (last accessed June 2018).

Kedar, S., B. Sturtevant, and H. Kanamori (1996). The origin of harmonic tremor at Old Faithful geyser, *Nature* **379,** 708–711.

Koper, K. D., and V. L. Hawley (2010). Frequency dependent polarization analysis of ambient seismic noise recorded at a broadband seismometer in the central United States, *Earthq. Sci.* **23,** 439–447, doi: 10.1007/s11589-010-0743-5.

Lin, F. C., D. Li, R. W. Clayton, and D. Hollis (2013). High-resolution 3D shallow crustal structure in Long Beach, California: Application of ambient noise tomography on a dense seismic array, *Geophysics* **78,** no. 4, Q45–Q56, doi: 10.1190/GEO2012-0453.1.

Schmandt, B., and R. W. Clayton (2013). Analysis of teleseismic *P* waves with a 5200-station array in Long Beach, California: Evidence for an abrupt boundary to inner borderland rifting, *J. Geophys. Res.* **118,** 5320–5338, doi: 10.1002/jgrb.50370.

Steeples, D. W., and R. D. Miller (1990). 1. Seismic reflection methods applied to Engineering, Environmental, and groundwater problems, *Geotech. Environ. Geophys.* 1–30, doi: 10.1190/1.9781560802785.ch1.

University of Utah (1962). University of Utah regional seismic network, *International Federation of Digital Seismograph Networks, Other/Seismic Network*, doi: 10.7914/SN/UU.

Wagner, G. S., and T. J. Owens (1996). Signal detection using multichannel seismic data, *Bull. Seismol. Soc. Am.* **86,** no. 1A, 221–231.

Wang, Y., F. C. Lin, B. Schmandt, and J. Farrell (2017). Ambient noise tomography across Mount St. Helens using a dense seismic array, *J. Geophys. Res.* **122,** 4492–4508, doi: 10.1002/2016JB013769.

Ward, K. M., and F. C. Lin (2017). On the viability of using autonomous three-component nodal geophones to calculate teleseismic *Ps* receiver functions with an application to Old Faithful, Yellowstone, *Seismol. Res. Lett.* **88,** no. 5, 1268–1278, doi: 10.1785/0220170051.

Wessel, P., and W. H. F. Smith (1991). Free software helps map and display data, *Eos Trans. AGU* **72,** 441–446.

Withers, M., R. Aster, C. Young, J. Beiriger, M. Harris, S. Moore, and J. Trujillo (1998). A comparison of select trigger algorithms for auto-

mated global seismic phase and event detection, *Bull. Seismol. Soc. Am.* **88,** no. 1, 95–106.

Withers, M. M., R. C. Aster, C. J. Young, and E. P. Chael (1996). High-frequency analysis of seismic background noise as a function of wind speed and shallow depth, *Bull. Seismol. Soc. Am.* **86,** no. 5, 1507–1515.

Wu, S. M., K. M. Ward, J. Farrell, F. C. Lin, M. Karplus, and R. B. Smith (2017). Anatomy of Old Faithful from subsurface seismic imaging of the Yellowstone Upper Geyser Basin, *Geophys. Res. Lett.* **44,** 10,240–10,247, doi: 10.1002/2017GL075255.

Xu, Y., K. D. Koper, and R. Burlacu (2017). Lakes as a source of short-period (0.5–2 s) microseisms, *J. Geophys. Res.* **122,** 8241–8256, doi: 10.1002/2017JB014808.

Jamie Farrell
Sin-Mei Wu
Kevin M. Ward
Fan-Chi Lin
Department of Geology and Geophysics
University of Utah
Salt Lake City, Utah 84112 U.S.A.
jamie.farrell@utah.edu

Published Online 4 July 2018